Engineering Structures 292 (2023) 116512

Contents lists available at ScienceDirect

Engineering Structures

journal homepage: www.elsevier.com/locate/engstruct

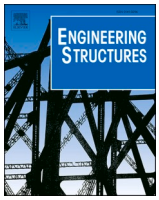

Experimental testing and structural analysis of composite tile – reinforced concrete domes

David López López [a,*], Ernest Bernat-Maso [b], Savvas Saloustros [c], Lluís Gil [d], Pere Roca [e]

[a] ETH Zurich, Department of Civil, Environmental and Geomatic Engineering, Switzerland
[b] Universitat Politècnica de Catalunya, Laboratory for the Technological Innovation of Structures and Materials, Spain
[c] École Polytechnique Fédérale de Lausanne, Earthquake Engineering and Structural Dynamics Laboratory, Switzerland
[d] Universitat Politècnica de Catalunya, Department of Strength of Materials and Engineering Structures, Spain
[e] Universitat Politècnica de Catalunya, Department of Civil and Environmental Engineering, Spain

ARTICLE INFO

Keywords:
Tile vault
Masonry
Formwork
Concrete shells
Numerical analysis
FEM

ABSTRACT

Conventional formworks for concrete curved shells either are expensive, complex and wasteful or have formal restrictions. Using tile vaults (also known as timbrel, Guastavino, thin-tile or Catalan vaults) as stay-in-place formwork for concrete shells could significantly reduce construction costs and material waste. Tile vaults only require formwork at the boundaries and provide a high formal flexibility.

The combination of masonry and reinforced concrete creates a new type of composite structure that needs experimental validation and new structural analysis models to deal with the specific features of the system. This paper presents experimental research on the component materials, load tests on doubly-curved, full-scale prototypes and the definition of a reliable Finite Element structural model for the analysis of the proposed hybrid structure.

The experimental research has involved the characterisation of the bricks, mortar, concrete and reinforcement composing the proposed system in order to provide the material properties to be considered in the structural analysis. The construction and testing of two composite sail domes in the laboratory have allowed the validation of the proposed FE model by comparing its predictions with the collapse mechanisms, damage, ultimate loads and load–displacement curves obtained experimentally.

1. Introduction

Tile vaults (also called timbrel, Guastavino, thin-tile or Catalan vaults) are traditional masonry structures built in layers using bricks and binder. The combination of a light brick (either a tile or a hollow brick) and fast-setting cement or gypsum allows the construction without the need of supporting formwork, except for the boundaries (Fig. 1) [1]. This made the construction technique inherently economic and, together with the low cost of the required materials, allowed its continued existence and spread during centuries [2–10].

After a period of partial abandonment in the second half of the 20th century [2], the tile vaulting technique has experienced a revival in the last two decades [11]. Different architects or engineers have found tile vaults worth to be recovered considering their efficiency, sustainability, aesthetics and the possibility, in many of the cases, to use local materials and workforce [12 13 14]. Furthermore, the formal versatility of the tile vaulting construction together with the advances in the computational tools for the design and analysis of masonry structures have allowed the construction of (so-called) free-form, funicular tile vaults [15 16]. These new, expressive structures came together with construction, design and materials innovations that provided affordable solutions despite the labour intensive nature of the technique [17 11 18].

The safety of masonry vaults has been traditionally analyzed by limit analysis [19] and the numerical implementations of the static (lower-bound) (e.g. [20–25]) and kinematic (upper-bound) (e.g. [26–29]) theorems. These approaches provide information related with the collapse mechanism and the force capacity. On the other hand, continuum [30–34] and discrete approaches [35–38] are preferred when information on the displacement capacity and damage evolution are of particular interest.

The possibilities and benefits of tile vaulting can be enhanced by combining it with reinforcement and/or concrete [39]. This

* Corresponding author.
E-mail address: david.lopez@ibk.baug.ethz.ch (D. López López).

https://doi.org/10.1016/j.engstruct.2023.116512
Received 28 February 2023; Received in revised form 29 May 2023; Accepted 19 June 2023
Available online 27 June 2023
0141-0296/© 2023 The Author(s). Published by Elsevier Ltd. This is an open access article under the CC BY license (http://creativecommons.org/licenses/by/4.0/).

combination has been explored in the past by architects or engineers seeking to improve the performance of the technique in terms of structural behaviour, economy or construction speed or easiness. The system studied in this paper, first presented in [40] and [41], learns from these experiences to propose a technique for a more sustainable and economic construction of concrete shells.

The use of tile vaults as integrated formwork for reinforced concrete could reduce the waste related to the construction of the conventional formwork, provide an unconventional, unique finishing to the intrados when left exposed, and offer an economically-competitive solution for many shapes and contexts. Furthermore, the tile vault does not only have a constructive and aesthetic purpose, but it is part of the structure as well (Fig. 2).

Apart from the authors' previous work [40 41], experimental and numerical research on composite structures involving tile vaults exists in the literature both with the purpose of restoring existing constructions and building new ones. The proposed systems are very different from the one presented in this paper. The work by Bertolesi *et al.* [42], aimed at the reparation of tile vaults, presents tests on two full-scale cross vaults strengthened with textile reinforced mortar. Subsequent research, by Bertolesi *et al.* as well [43], performs numerical modelling of those specimens, both before and after the application of the reinforcement. Dejong *et al.* [44] and Ramage and Dejong [45] tested and analysed geogrid-reinforced timbrel vaults envisaging their construction in seismic areas and used the system in different architectural projects [18 46]. A similar approach was followed by Castori *et al.* [47,48], who tested seventeen tile-vaulted arches strengthened with a glass fibre reinforced polymer (GFRP) mesh. The variables differentiating the seventeen specimens were the application or not of the mesh, its position (either only between the layers or also on the extrados), the mortar type and the number of layers composing the arches. A GFRP mesh has also been recently used by Savino et al. [49] to reinforce the specimens they used for the testing and numerical analysis of Catalan vaulting using earth-based bricks called "Ecorrasillas".

Recent research has revealed relevant architectural pieces featuring tile vaults in Cuba [50], where the National Art Schools in Havana are a striking example [51]. The work by Douglas *et al.* [52,53] and Hughes *et al.* [54,55] analyses existing reinforced composite tile-concrete ribbed domes in these Cuban art schools. The ribs of the dome did not allow the traditional construction without supporting formwork, which entails a significant difference with the system proposed in the present paper, not only in terms of the construction process and economy, but also in relation to the structural performance considering their different cross-section [51]. The domes are assessed using Finite Element Analysis: a linear elastic analysis in the case of the work by Douglas *et al.* [52] and a nonlinear analysis using a concrete damage plasticity model with an effective-section approach (applying a simplified cross-section, lumping the tile vault and reinforced concrete in a single material) in the case of Hughes *et al.* [54].

A lower-bound method for the structural design and analysis of composite tile vault-reinforced concrete shells was presented in López López *et al.* [56]. The method is based on Thrust Network Analysis [57], but takes into account the tensile capacity of the reinforcement and the limited compressive strength of the masonry and concrete by computing a virtual thickness within which the thrust network must be contained to guarantee a global stability of the hybrid structure.

Despite the mentioned previous work on the field, the tile vault and the reinforced concrete, combined as shown in Fig. 2, create a new hybrid structure that still requires numerical and experimental research to fully understand the specific structural features of the system. This paper addresses this issue by presenting the definition of a Finite Element (FE) structural model for the analysis of the proposed composite structure. Furthermore, the calibration of the FE model is carried out by comparing its results with those provided by physical tests on the system. The experimental research described in this paper has contributed to the understanding of the system's structural behaviour, and has allowed further validation of the feasibility of the construction technology and its application to doubly-curved vaults. This validation has been achieved by building and load-testing two composite sail domes. In addition, the experiments carried out can serve as benchmark for eventual further structural models. The research has also involved the characterisation of the materials composing the shells (bricks, mortar, concrete and reinforcement).

The characterization of the composite structure's materials is described in Section 2, followed by the load tests on sail domes in Section 3. The work related to the Finite Element Method (FEM) is presented in Section 4, which includes the description of the modelling technique utilized, the adopted material properties and the analysis of the tested specimens. The last section is Section 5, devoted to present the conclusions.

2. Material characterization

The materials used for the construction of the sail domes' masonry were also used for the construction of further prototypes and samples in the context of a wider research project conducted at ETH Zurich, Switzerland, and Universitat Politècnica de Catalunya, Spain. A detailed description of the masonry characterization, including values of the individual materials (tiles, fast-setting cement and Portland cement mortar), can be found in [40] and [41] and is summarised in Tables 1 and 2. The values are obtained from experimental tests performed according to EN 1015 [58] and EN 12390 [59] and calculated using equations provided by Eurocode 6 [60] and the Spanish concrete code EHE [61]. The compressive strength of the masonry was estimated as described in [40] for a two-layered tile vault with a thickness of 36 mm. The tiles' dimensions are 277 × 134 × 14 mm and each has a weight of

Fig. 1. Construction of tile vaults without supporting formwork [1].

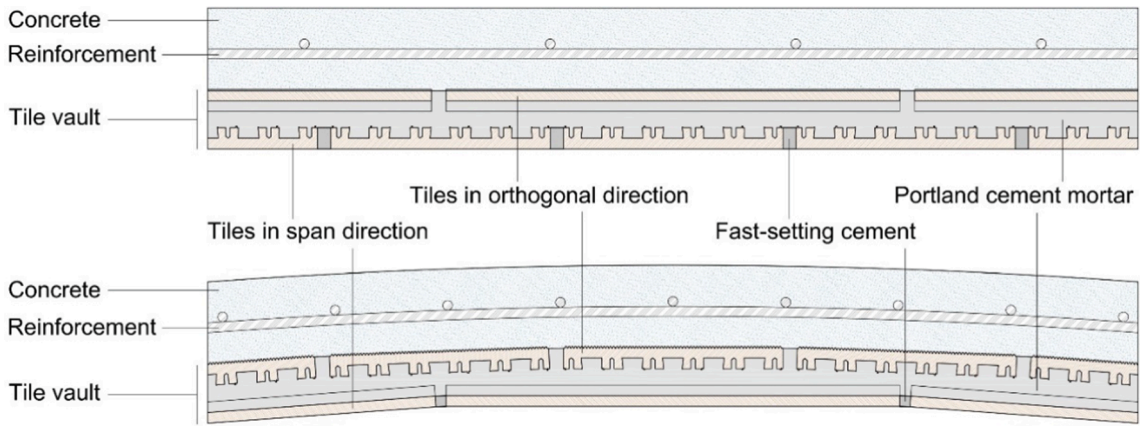

Fig. 2. Cross-sections of a barrel vault using the proposed construction system. Top) Transversal cross-section, bottom) longitudinal cross-section. [41].

Table 1
Properties of the materials composing the masonry.

Tiles				Fast-setting cement				Portland cement mortar			
Compressive strength				Compressive strength		Flexural strength		Compressive strength		Flexural strength	
Extrusion direction		Orthogonal direction									
N/mm^2	Coef. Variat. %	N/mm^2	Coef. Variat. %	N/mm^2	Coef. Variat. %	N/mm^2	Coef. Variat. %	N/mm^2	Coef. Variat. %	N/mm^2	Coef. Variat. %
111	8.93	87	2.70	4.47	10.16	0.9	1.48	6.98	14.72	2.5	8.47

Table 2
Material properties of the masonry.

Masonry			
Compressive strength N/mm^2	Flexural strength N/mm^2	Tensile strength Coef. Variat. %	N/mm^2
13.02	4.47	8.54	1.89

800 g. The densities of the materials are 1373 kg/m^3 for the fast-setting cement, 1940 kg/m^3 for the Portland cement mortar and 2000 kg/m^3 for the masonry.

The concrete poured on top of the tile dome had a density of 2460 kg/m^3 and its mix proportions are shown in Table 3.

Compression tests were performed on 200-mm-high, 100-mm-diameter, concrete cylinders according to EN 12390 [59]. The resulting average compressive strength was 33.4 N/mm^2 with a coefficient of variation of 3.92%.

The reinforcement used to complete the composite structure consisted of 6-mm-diameter steel bars. Ten specimens were tested in tension following EN ISO 15630–1 [63], resulting in a mean tensile strength of 581 N/mm^2 and a Young's modulus of 207000 N/mm^2, with respective coefficients of variation of 0.95 % and 3.61%.

Compression and bending tests were performed on composite samples to test the bonding between the masonry and the concrete layers [64]. The samples tested in compression had sizes of 134 × 136 × 86 mm and were composed of the masonry element (36 mm in total) and the concrete layer (50 mm). The samples tested in bending had sizes of 564 × 277 × 86 mm, including also masonry (36 mm) and concrete (50 mm). The tests showed sufficient bonding between the masonry and the concrete, with debonding happening only after a drop of 20% of the force capacity.

Table 3
Concrete's mix proportions.

Cement CEM I 42.5 N-SR 5 [62]	Water	Sand<4 mm	Gravel5 mm < x < 12 mm	Limestone filler	Super-plasticizer MasterGlenium ACE425, BASF
kg	kg	kg	kg	kg	kg
1	0.5	2.877	2.324	0.332	0.01

While further research specifically focused on the bond strength between tiles and concrete is necessary, existing studies on masonry bond can provide valuable insights into strategies for enhancing the structural performance of the proposed composite technique in this aspect [65,66]. The factors influencing masonry bond, such as mortar composition, masonry unit characteristics, and environmental conditions, can serve as initial guidelines for improving the bond strength between tiles and concrete. By considering these factors and adapting the findings from masonry bond research, it is possible to develop strategies that may optimize the tile-concrete bond and enhance the overall structural performance of the composite technique [41].

In terms of mortar composition, enhancing the flexural bond strength can be achieved by increasing the amount of cement in the mix design and using mortars with higher strength values [67]. The addition of lime or soil to the mortar mix has also been found to improve bond strength [66–68].

Regarding masonry unit characteristics, the moisture content at the time of laying plays a significant role in bond strength. Partially wetted bricks tend to exhibit better bond development compared to dry or completely saturated bricks [66–69]. Additionally, the surface texture of the brick is important, with bricks featuring a larger frog area demonstrating better bond performance [68,70].

Environmental conditions should also be taken into account. Curing conditions have an impact on bond strength, and proper curing techniques should be employed to optimize bonding. During mortar placement, applying the appropriate pressure is crucial to ensure proper adhesion between the mortar and masonry unit. Additionally, attention should be given to filling the frog or valleys on the unit's surface adequately, as this contributes to enhancing bond strength [71–73].

3. Load tests on sail domes

3.1. Dome's geometry and test configuration

The two identical sail domes are squared in plan and are supported on the corners. They are spherical, have an intrados radius of 2 m, a rise of 0.39 m and a span of 1.76 m.

A minimal thickness of the construction system is sought. A self-supporting tile vault requires at least two courses of bricks. The minimum thickness of such structure is 36 mm, using 14-mm-thick tiles and applying 8-mm-thick mortar joints. The concrete layer is also built with minimal thickness considering an exposure class with no risk of corrosion or attack (X0), a cast on an uneven surface and allowing small design deviations of 4 mm [74], resulting in a concrete cover of 19 mm on both sides. According to this, the cross-section consists of a 36-mm-thick tile vault and a 50-mm-thick concrete layer with the reinforcement placed at mid concrete thickness. The reinforcement consists of 6-mm-diameter steel bars at 70 mm in both directions (Fig. 3). Among the various options available, the size of the rebars was selected to ensure ease of construction in terms of bending and positioning. This choice was made not only for the building of the tested domes, but also with the foresight of potential future construction involving more intricate shapes.

Regarding the total thickness of the cross-section, 86 mm, two facts can be pointed out: i) the ratio span/thickness of the structure is low, i.e., larger structures could be built using this cross-section provided the tile vault withstands construction loads such as a worker, material, tools or wet concrete on top of it; ii) considering other situations with a less favourable exposure class and higher design deviations, a larger concrete cover may be required.

The domes' supports lie on a steel frame, to prevent their displacement and to allow transportation. These consist of four prefabricated concrete blocks positioned on the four corners of the steel frame (Fig. 4), on which the dome is simply supported. Once the specimen is moved to the test position, the steel frame is used to tie the corners of the structure in order to prevent or minimize possible displacements at the supports.

A squared, 160-mm-sided, horizontal surface made of concrete receives the load at one quarter of both span directions (Fig. 5). A single actuator applies a displacement-controlled punctual load at a speed of 0.2 mm/min distributed to the square surface through a 20-mm-thick, 170-mm-sided, squared steel plate. The loading device is a hydraulic quasi-static HIDRASA actuator of 300 kN of force range and 500 mm of displacement range. Data is acquired with an HBM MGCPlus acquisitor at 50 Hz. The use of a point load instead of a distributed one (e.g., using sand bags) was motivated for three reasons. First, it allowed to apply a displacement-controlled load, making possible the investigation of the post-peak response. Second, it permitted a better control of the position and amount of load, which was important for the numerical modelling of the test. Third, the use of sand bags would increase discretely the load, whereas with the used setup, a continuous displacement (and thus load) variation could be applied.

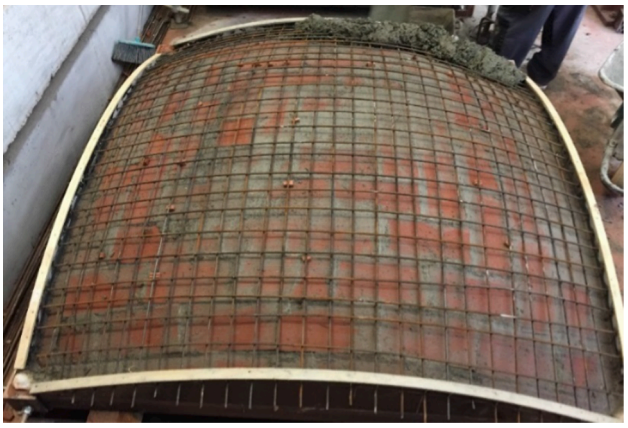

Fig. 3. Reinforcement of the sail dome under construction.

Fig. 4. Corner of the steel frame with a prefabricated concrete piece on which the dome was simply supported.

Seven potentiometers (100 mm range and 0.2% linearity) are used to measure vertical displacements as shown in Fig. 5. Although the setup is planned to prevent the displacements of the supports, one LVDT (20 mm range and 0.2% linearity) measuring horizontal displacements is installed with the purpose of verifying that those displacements are negligible (Fig. 5, H1).

Two expert bricklayers and one helper required three working days to build the two domes, which roof a total surface of 6.6 m^2. During the first and second days, the tile domes were finished and the reinforcement placed. The third day was devoted to the concrete placement, to the building of the loading platforms and to the preparation of the control specimens.

3.2. Results

The tested sail domes had a non-linear plastic behaviour with long post-peak unloading responses. The peak loads were 91.3 kN and 94.3 kN for the composite domes 1 and 2, respectively (Fig. 6). The ultimate loads were significantly higher than those required in Eurocode 1 [75] for concentrated loads in any of the categories of use, where the highest recommended value intended for determination of local effects is 7 kN. For both prototypes, the test ended when the corner opposite to the loading point detached and slipped upwards from the support (Fig. 7). Small upwards displacements of that corner in relation to the support were also detected visually after the peak load and before the end of the tests.

The cracks and crack patterns identified during the load tests (Fig. 8), together with the registered displacement data, allow the identification of the failure mechanism, which was the same for both domes (Fig. 9). A crack at the tile vault under the actuator running perpendicular to the dome's sides, developed from the loading point to the closest edges, evidenced the appearance of a hinge under the load (Fig. 9, d). Crushing of the concrete was reported at this hinge in the last part of the test, after the development of the collapsing mechanism. Cracks at the corners also manifested the hinges at the supports (Fig. 9, e and f, and Fig. 10). A group of cracks on a portion of the concrete surface revealed the creation of the last hinge (Fig. 8 and simplified in Fig. 9, g).

The data registered by the potentiometers (Fig. 11 and Fig. 12) are in accordance with the assumed mechanism, illustrated in Fig. 9. Measured points P1 (under the load) and P3 (the closest one to the hinge under the load) suffered the biggest displacements, whereas P5 and P7 registered the smallest ones, with almost no displacement during the loading phase. The latter were also the only points registering upwards

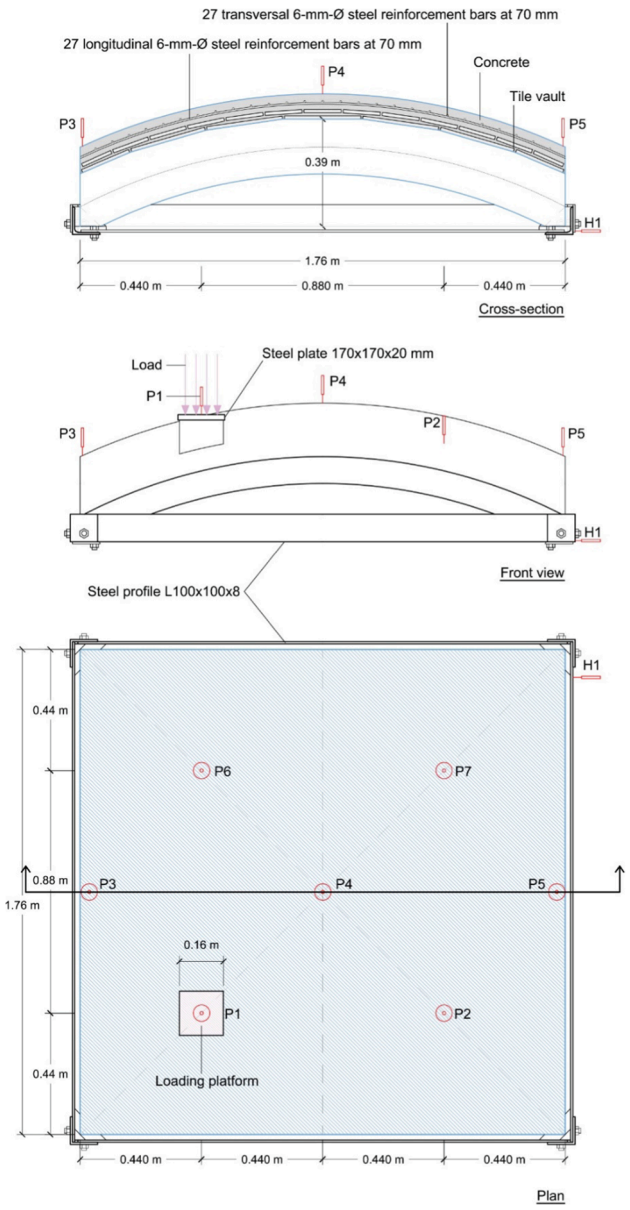

Fig. 5. Setup of the monitoring and load test for the composite sail domes. Potentiometers indicated as P1 to P7. Top) cross-section, middle) front view, bottom) plan.

displacements after the development of the mechanism, which is in accordance with their position in block 3 of Fig. 9, c. The points P2, P4 and P6 had moderated downwards displacements, also in concert with their position in block 2 of Fig. 9, b. The data measured by potentiometers P2 and P6 at the composite sail dome 1 (Fig. 11) had to be discarded for the first part of the tests (below a load of 70 kN) due to an imperfect adhesion of the sensor to the concrete's surface. LVDT H1 (Fig. 5) registered displacements at the peak load of 0.49 mm and 0.58 mm for composite dome 1 and 2 respectively.

Small cracks at the interface masonry-concrete were reported at the last fraction of the loading phase, from approximately 85% of the peak load. During the post-peak unloading response, a gradual detachment of the bricks from the concrete layer was visible at the four corners until some portions of the tile vault fell (Fig. 13). After the detachment of the tile vault from the concrete at the corner next to the loading point, compression cracks appeared at the concrete's upper surface running from the loading platform to the mentioned corner (Fig. 8).

3.3. Comparison with an unreinforced tile vault

Two identical plain, unreinforced tile-vaulted shells (Fig. 14) were subjected to load-tests [76], similar to the ones described earlier. These new domes can be seen as the outcome of removing the concrete layer and slightly repositioning them upwards, aligning their central surface with the axis of the composite shells. Fig. 15 illustrates the geometry of the vaults, as well as the setup of the load test and the monitoring system. The loading device and the potentiometer used in the first set of load tests were also employed in this case.

The tested specimens' peak loads were 19.5 kN and 21.0 kN, resulting in an average ultimate load of 19.75 kN. The inclusion of a 50-mm-thick concrete layer on top of the 36-mm-thick masonry structure led to a significant 469% increase in the loading capacity when compared to the analysed composite shells.

4. Finite element method

This section proposes the use of a FEM technique for the analysis of the proposed composite structure, describing the modelling technique and the adopted material properties. The ductile post-peak response and the extended damage distribution of the tested composite vaulted system have motivated the use of a continuum finite element approach. Its validity is demonstrated by comparing the outcome of the tested specimens' analysis with the experimental results in terms of collapse mechanisms, damage, ultimate loads and load–displacement curves.

The material and geometrical nonlinear analysis is carried out using the software DIANA FEA [77].

4.1. Modelling technique utilized

4.1.1. Description of the geometry

The finite element model presented in this section corresponds to the composite sail dome described in Section 3, whose geometry is shown in Fig. 5. The concrete loading platform and the steel plate are also modelled in order to apply a displacement at the top centre of the plate and replicate the real conditions as faithfully as possible (Fig. 16).

Regarding the boundary conditions, the four concrete supports on which the dome is simply supported are also modelled. An interface between the supports and the dome is modelled to allow the detachment of the contact surface as a consequence of the formation of the hinges (Fig. 17, right). In addition, the four support are provided with springs in the X and Y directions to allow for the small horizontal displacements registered during the load tests (Fig. 17).

The composite dome, the loading platform and the steel plate are modelled using a four-node, three-sided, isoparametric, solid tetrahedral element. The reinforcement bars are modelled as lines embedded in the solid elements, as indicated in DIANA FEA [77]. The interface between the shell and the concrete supports is modelled using interface elements between two planes in a three-dimensional configuration, based on linear interpolation and with a 3-point integration scheme [77]. The concrete supports are modelled using a six-node isoparametric solid element.

The number of finite elements of the dome's concrete layer is 160053, whereas that of the tile vault is 110231. These elements have an approximate average edge size of 2 cm. Each concrete support has 74 elements and each of the four interfaces has 37 elements. Every support has 29 of its nodes connected to two spring elements, in the *X* and in the *Y* direction, making a total of 232 spring elements.

4.1.2. Material modelling

Masonry is simulated as a homogeneous isotropic material with average properties using a total strain crack model [77 78]. This smeared crack model features a predefined tension softening exponential function based on fracture energy and a compressive behaviour following a parabolic curve, which in DIANA is a formulation based on

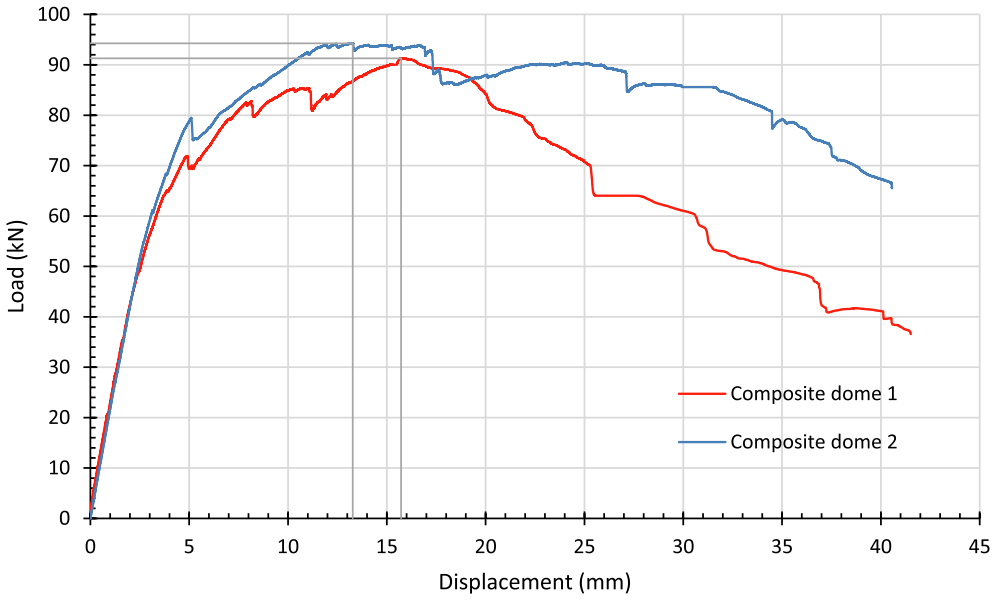

Fig. 6. Ultimate load test. Load-displacement curves of the two composite sail domes at the loading point.

Fig. 7. Detachment and upwards displacement of the support opposite to the loading point.

fracture energy according to Feenstra [79 77].

The concretés constitutive model is also a total strain crack model. The nonlinear material model for the steel reinforcement is based on Von Mises plasticity, using the Von Mises yield criterion and no hardening function. A discrete cracking model is used to define the relation between stresses and relative displacements across the interfaces. A brittle behaviour is chosen for tension, with which a full reduction of the tensile strength is applied after the introduced strength limit is surpassed [77].

As the experimental results showed that separation between masonry and reinforced concrete was not critical and occurred after a drop of 20% of the force capacity (i.e., after what is considered the displacement capacity of the vault), a discrete modelling of the interface between the two materials was not considered. This choice allows for a more efficient numerical simulation without compromising the accuracy.

Linear elastic properties are assigned to the springs and the steel plate on top of the loading platform.

Fig. 8. Cracks on the extrados of the composite sail dome 1 after the test.

4.2. Adopted material properties

Different strategies have been used to obtain the material properties of the tile vault, namely, experimental tests, using expressions provided in codes and using values extracted from related literature.

Following previous analysis of brick masonry structures, the Poisson's ratio is taken as 0.2 (as for instance in Saloustros [80]).

A curved (faceted) structure built with straight masonry units features unavoidably slight variations of its thickness. The construction of the composite sail domes maintained the centre of the tiles' lower face in the first course tangent to a fictitious spherical intrados, and the centre of the tiles' upper face in the second course tangent to a fictitious spherical extrados. Due to this fact and for the presented composite sail dome's geometry and tile's sizes, the tile vault in this case had a maximum thickness of 36 mm, which decreased 4.8 mm at the intrados' joints (Fig. 18). The tile vault's thickness is therefore taken as the resulting 31.2 mm for calculation purposes. A thickness reduction of the two-layered tile vault means a thickness decrease only of the mortar

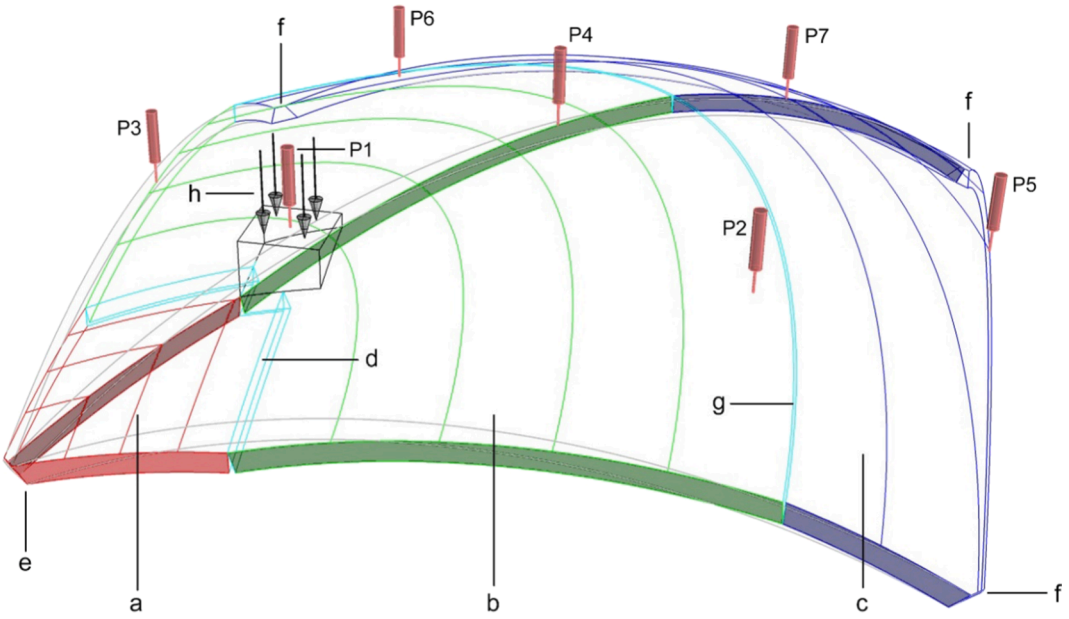

Fig. 9. Simplified scheme of the tested sail domes' failure mechanism, a) block 1 (red), b) block 2 (green), c) block 3 (blue), d) hinge under the load, e) hinge at the load's closest support, f) hinge at the rest of the supports, g) hinge at the extrados, and h) load. Hinge g has appeared in the experiment as a series of distributed cracks.

Fig. 10. Crack at the support closest to the loading platform.

layer between the tiles. This has an influence in the masonry's mechanical properties, which need to be recomputed [40]. Considering the corrected thickness, the density results in 2009 kg/m^3, whereas the compressive strength results in 13.95 N/mm^2 using the following equation in Eurocode 6 [60] as described in [40]:

$$f_k = K f_b^{0.7} f_m^{0.3} \tag{1}$$

where K is a constant, and f_k, f_b and f_m are, respectively, the tile vault's characteristic compressive strength, the normalised mean compressive strength of the units and the mortar's compressive strength; the three of them in N/mm^2.

The compressive fracture energy, G_{fctv}, equal to 20.30 N/mm, is obtained using the expression from the Model Code 90 [81], as proposed in Lourenço [82], which is applicable for a concrete's compressive strength, f_c, between 12 and 80 N/mm^2:

$$G_{fc} = 15 + 0.43 f_c - 0.0036 f_c^2 \tag{2}$$

The tensile fracture energy, G_{ftv} equal to 0.032 N/mm, is also obtained from concrete's recommended values in the Model Code 90 [81] and is derived from the following expression:

$$G_f = G_{Fo}(f_c/10)^{0.7} \tag{3}$$

where G_{Fo} is the base value of fracture energy and is equal to 0.025 provided that the maximum aggregate size is 8 mm.

As described in Section 2, the tensile strength is equal to 1.89 N/mm^2. The values of the tile vault's Young's modulus, 8500 N/mm^2, and shear retention, 0.05, are extracted from López López [64], where a tile vault FE model is calibrated using the results of the experimental tests on full-scale tile-vaulted prototypes [76]. The adopted material properties for the tile vault are summarized in Table 4.

The concrete used to build the composite sail domes was also used for the construction of the loading platforms and the supports. As reported in Section 2, it had a density of 2460 kg/m^3 and a compressive strength of 33.4 N/mm^2. The Poisson's ratio is taken as 0.2 (Eurocode 2 [74]) and the elastic modulus results in 31590 N/mm^2 using the following equation from the Eurocode 2:

$$E_{cm} = 22[(f_{cm})/10]^{0.3} \tag{4}$$

where the compressive strength, f_{cm}, is expressed in N/mm^2. The compressive fracture energy is computed using Equation (2) and results in 25.35 N/mm.

The concrete's tensile strength and tensile fracture energy, together with the springs' stiffness, are the values used to calibrate the model.

Two steel materials are defined and assigned to the reinforcement bars and to the plate on top of the loading platform. Regarding the steel material applied to the rebars, the density and the Poisson's ratio are taken respectively as 7850 kg/m^3 and 0.3 [83]. The Young's modulus and the tensile strength were obtained through the experimental research described in Section 2 and resulted in 207000 N/mm^2 and 581 N/mm^2 respectively. The material properties of the steel assigned to the rebars are summarized in Table 5.

The elastic material properties assigned to the steel plate on top of the loading platform are a Young's modulus of 210000 N/mm^2 and the same values for the Poisson's ratio and density as in the steel material assigned to the reinforcement bars.

The material properties used to define the selected interface element are the normal and shear stiffness and the tensile strength. The normal

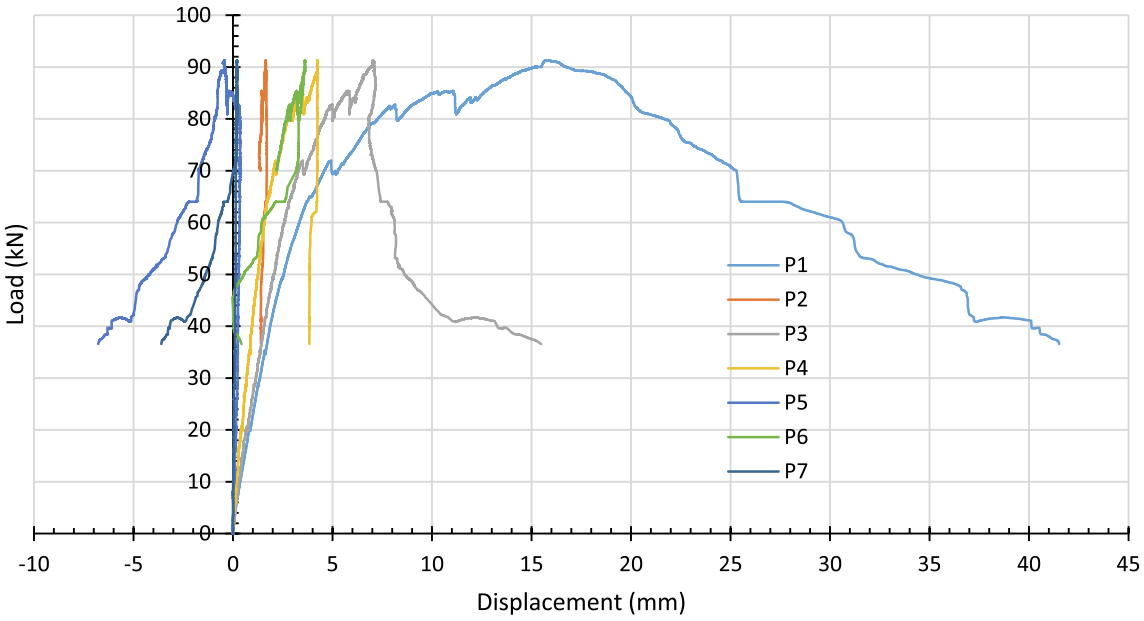

Fig. 11. Load-displacement curves of the composite sail dome 1.

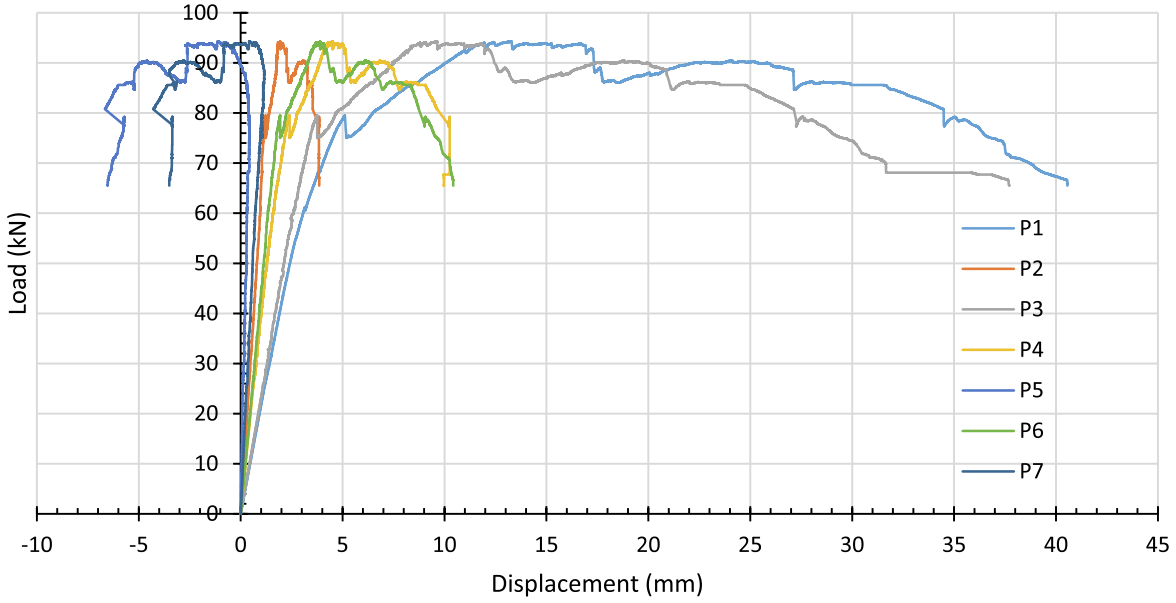

Fig. 12. Load-displacement curves of the composite sail dome 2.

and shear stiffness, K_n and K_s, are estimated using the following equations, as proposed in Červenka *et al.* [84]:

$$K_n = \frac{E}{t} \tag{5}$$

$$K_s = \frac{G}{t} \tag{6}$$

where E and G are the elastic and shear moduli of the surrounding material and t is the thickness of the interface, which is here taken as 10 mm [84]. The obtained normal stiffness is 3159 N/mm^3, whereas the shear stiffness results in 1316 N/mm^3, adopting a concrete's shear modulus of 13162 N/mm^2, derived from the expression in Model Code 90 [81],

$$G = \frac{E}{2(1+\nu)} \tag{7}$$

The tensile strength of the interface is taken equal to the tensile strength of the concrete and, as mentioned above, is used as a variable for the calibration of the model.

4.2.1. *Calibration of the model*

The model has been calibrated by gradually updating the springs' stiffness and the concrete's tensile strength and tensile fracture energy until a satisfactory agreement between the numerical and experimental load–displacement curves was obtained. Slight displacements of the supports have a meaningful influence in the results of a finite element analysis. The springs in the model allow the replication of the supports' small displacements registered during the load tests. The modification of the springs' stiffness has a clear influence in the slope of the

Fig. 13. Intrados of the composite sail dome 1 after the test showing debonding between the tile vault and the concrete layer at the corners.

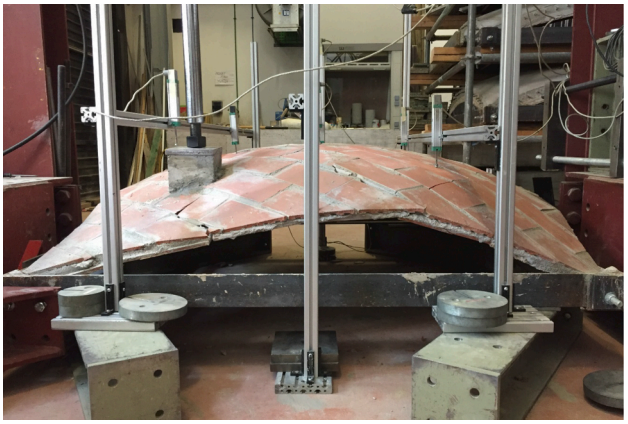

Fig. 14. Load test setup of the plain, tile-vaulted sail domes.

load–displacement curves. These slopes from the experimental research, together with the registered maximum horizontal displacement at H1 (Fig. 5), have been used as reference for the calibration of the springs' stiffness. Further work on this subject might include a sensitivity analysis to further assess and quantify the influence of the supports' horizontal displacements on the stiffness and ultimate load of this kind of structures. Load tests on prototypes with different geometries and allowing different supports' horizontal displacements could be relevant regarding this objective.

The properties concerning the non-linear tensile behaviour of the concrete, namely tensile strength and tensile fracture energy, have also been the values used to calibrate the model. The modification of these values had a direct influence, among others, in the resulting peak load.

The adopted material properties for the concrete after the calibration of the model are summarized in Table 6.

4.3. Analysis of tested specimens

The finite element analysis carried out on the domes model considered geometrical and material nonlinearity, using the Regular Newton-Raphson iteration scheme [77].

After the calibration process, the proposed FE model is able to replicate the behaviour of the tested specimens in terms of stiffness, peak load, displacements, cracks and failure mode. The FE model's load–displacement curve at the loading point in Fig. 19 shows a close approximation to the structural behaviour of the built composite domes with a similar slope at the first stretch of the plot and a peak load, 91.94 kN, in between the two peak loads registered during the experimental tests, which attained values of 91.29 and 94.26 kN for the first and the

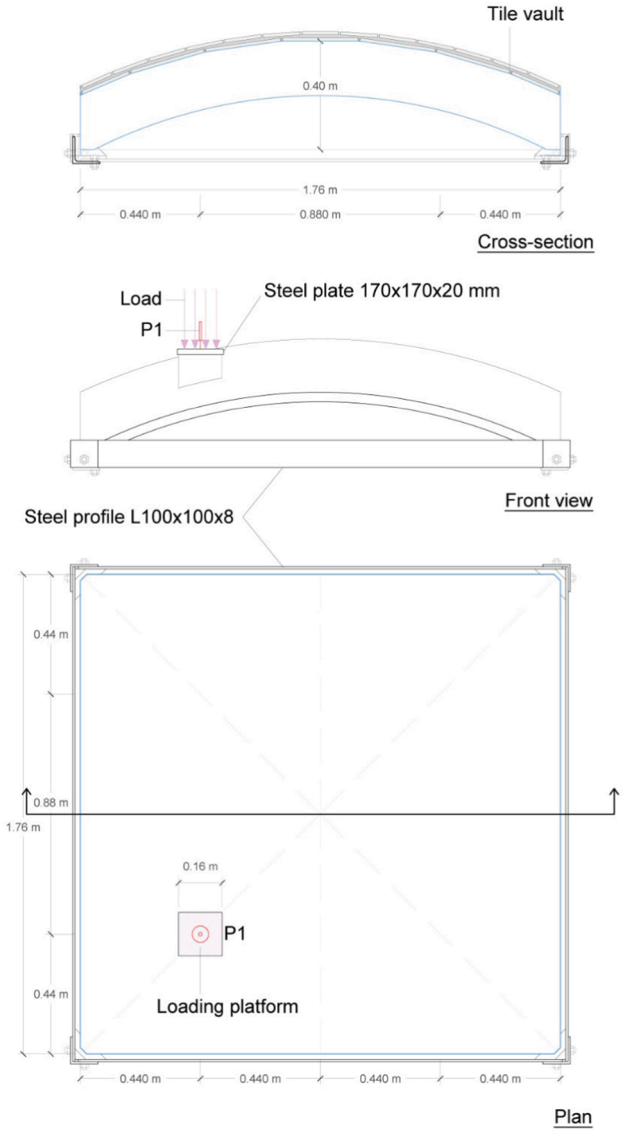

Fig. 15. Setup of the monitoring and load test for the plain, tile-vaulted sail domes. Potentiometer indicated as P1. Top) cross-section, middle) front view, bottom) plan.

second composite domes respectively.

The numerical model's horizontal displacement at H1 (Fig. 5) at the peak load is 0.57 mm and is as well in accordance with the experimental tests, which resulted in 0.49 mm and 0.58 mm for composite domes 1 and 2 respectively. The LVDT measuring the displacement at H1 was placed in contact with the frame's steel profile that linked the two corresponding contiguous supports. This profile was not included in the FE model and this displacement could therefore not be directly measured from it. Alternatively, this value was obtained by measuring the displacement of a central point of the two mentioned contiguous supports in the direction of the installed LVDT. Knowing the distance of H1 to these two supports, the displacement can then be easily calculated.

The use of interface elements between the dome and the concrete supports has enabled to simulate the hinges and the detachment of the supports reported during the load tests. In particular, the displacements of the FE model at an early stage of the loading process shown in Fig. 20 illustrate the detachment of the upper part of the support closest to the loading platform, which was visually reported as the crack featured in Fig. 10. The detachment and upwards displacement of the support documented in Fig. 7 is also reproduced by the numerical model

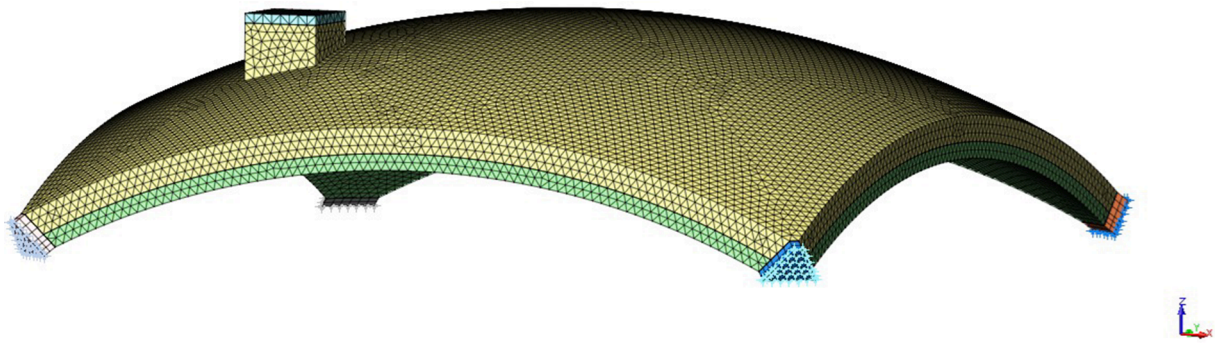

Fig. 16. Meshed geometry of the composite sail dome.

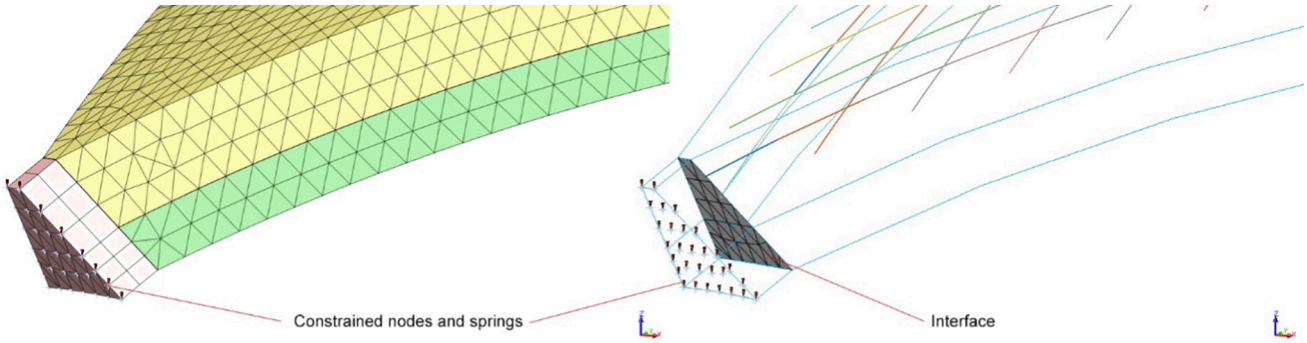

Fig. 17. Concrete support of the composite dome's model. Left) meshed geometry showing the vertically constrained nodes on which springs in X and Y directions are applied, and right) interface between the concrete support and the dome.

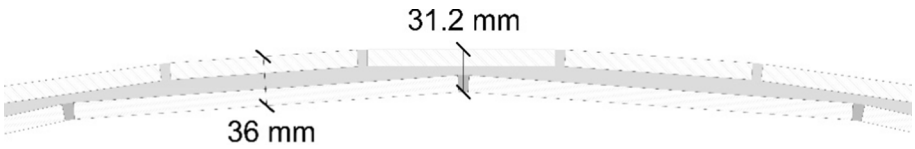

Fig. 18. Cross-section of the tile-vaulted part of the sail dome indicating its maximum and minimum thickness.

Table 4
Tile vault's adopted material properties.

Young's modulus	Poisson's ratio	Density	Comp. strength	Comp. fracture energy	Tensile strength	Tensile fracture energy	Shear retention
E	ν	ρ	f_{ctv}	G_{fctv}	f_{ttv}	G_{fttv}	β
N/mm^2	–	kg/m^3	N/mm^2	N/mm	N/mm^2	N/mm	–
8500	0.2	2009	13.95	20.30	1.89	0.032	0.05

Table 5
Steel rebars' material properties.

Young's modulus	Poisson's ratio	Density	Tensile strength
E	ν	ρ	Ft
N/mm^2	–	kg/m3	N/mm^2
207,000	0.3	7850	581

(Fig. 21) and signals the end of the analysis at a displacement of 18.96 mm of the loading point. This coincides approximately with the first small upwards slip of that support reported in the load test of the composite dome 2.

It is worth pointing out that this detachment is partly due to the particular type of boundary conditions, simply supported and specifically designed for the laboratory context. A common support detail solution for concrete shells in real practice would be a fixed one with overlapping reinforcement bars embedded both in the shell and in the

Table 6
Concrete's material properties.

Young's modulus	Poisson's ratio	Density	Comp. strength	Comp. fracture energy	Tensile strength	Tensile fracture energy
E	ν	ρ	f_{cc}	G_{fcc}	f_{tc}	G_{ftc}
N/mm^2	–	kg/m^3	N/mm^2	N/mm	N/mm^2	N/mm
31,590	0.2	2460	33.40	25.35	0.334	0.01

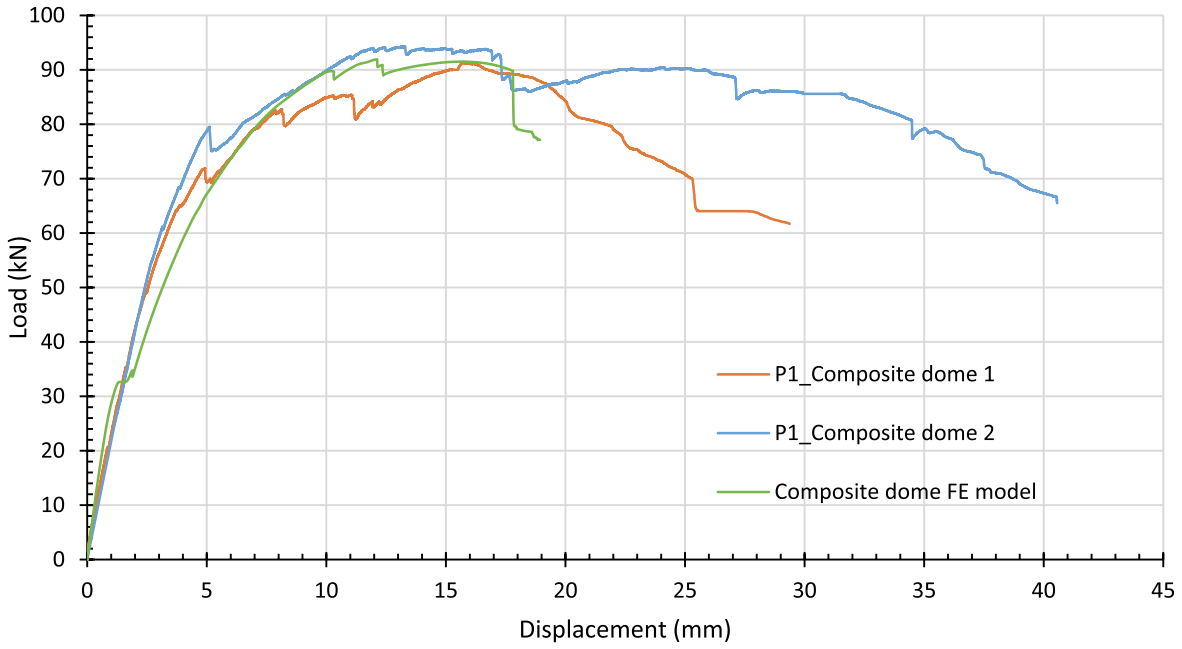

Fig. 19. Load-displacement curves at the loading point (P1, Fig. 5) of the two composite domes and the corresponding FE model.

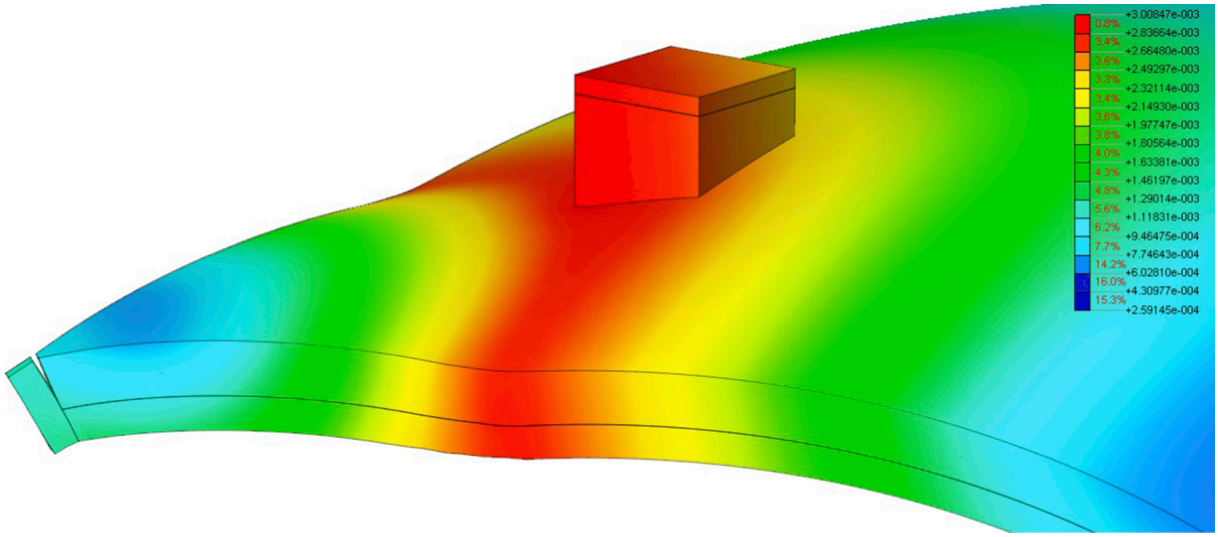

Fig. 20. FE model of the composite dome. Displacements (m) at a load of 44.72 kN. Detail of the detachment of the support closest to the loading point.

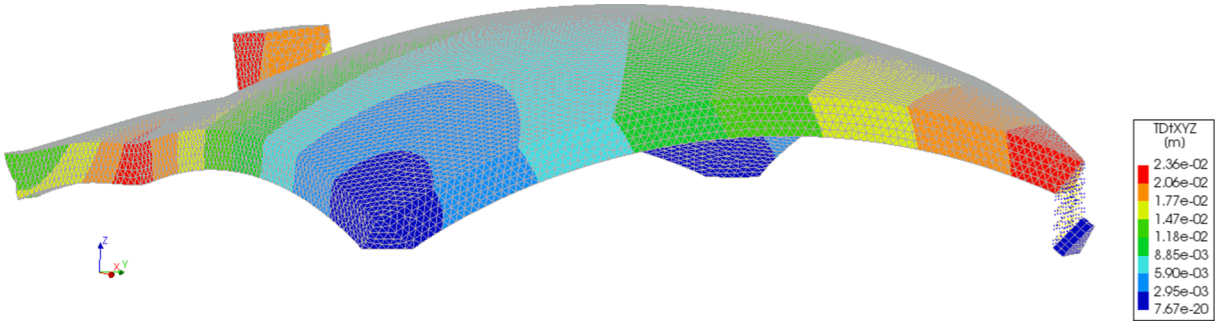

Fig. 21. FE model of the composite dome. Displacements (m) at the last loading step showing the detachment and upwards displacement of the support opposite to the loading point.

support.

Apart from the detachments and displacements at the supports, the model also recreates the two main sets of cracks detected during the load tests, namely, the ones on the intrados related to the formation of the hinge under the load (Fig. 22, left) and the radial-patterned cracks on the concrete's surface at the extrados (Fig. 22, right).

5. Conclusions

The construction of the full-scale, sail-dome prototypes demonstrated the feasibility of the proposed technique to build doubly-curved composite shells using tile vaults as stay-in-place formwork for reinforced concrete. Furthermore, the ultimate loads registered at the tests, higher than those required by the codes, demonstrated satisfactory structural behaviour. By testing unreinforced tile-vaulted domes, as well as composite ones, it was observed that the ultimate load of the 36-mm-thick masonry shell increased by 469% upon the addition of the 50-mm-thick concrete layer.

The tested specimens demonstrated a satisfactory bond between the tile vault and the concrete layer. However, to achieve a stronger bond, several strategies can be employed. One approach is to design the concrete mix with specific proportions of cement and additives tailored to enhance bonding properties. Additionally, ensuring an optimal level of moisture in the tiles during the construction process promotes better adhesion. Furthermore, using tiles or bricks with a larger frog area increases the contact area between the tile vault and the concrete layer, leading to a stronger bond.

Although specimens with specific cross-section sizes are presented in this paper, the construction system's thickness proportions between the tile vault and the concrete layer may be adapted to the particular design, construction and structural requirements (span, loads, geometry, etc.). In this regard, the dimensioning of the masonry layer should be carried out taking into account both the finished state with a fully-operational, composite cross-section, but also the temporary condition of the tile vault serving as formwork for the reinforced concrete. Additionally, the diameter of the reinforcement steel bars should be selected considering not only their structural performance, but also taking into account construction restraints, namely their capacity to adopt the shape of the shell and their ease of placement.

The load tests on the composite sail domes showed a collapse mechanism featuring hinges. In contrast to unreinforced masonry shells, and as a result of the reinforcement's contribution, the hinge at the extrados becomes a "distributed hinge", which is accompanied by a cluster of visible cracks on the concrete surface. Furthermore, the presence of reinforcement significantly influences the structural behaviour of the system in comparison to plain masonry by adding a desired ductility and therefore avoiding an eventual brittle collapse. Seeking that purpose, the structure should be designed avoiding over- or under-reinforced cross-sections. The software ELARM facilitates this design process specifically for this kind of composite structures [40,41,56].

The monitoring of the load tests on the full-scale prototypes, together with the characterization of the materials involved, allowed the calibration of the FE structural models and provide an important benchmark for further research on the structural behaviour of these composite structures. The presented FE models replicated accurately the overall structural behaviour of the analysed specimens, including stiffness, peak load, collapse mechanism, displacements and cracks' position.

The FE analysis of the tested specimens showed a high sensitivity of the models to slight displacements of the supports. The monitoring of the support's horizontal displacements, even if they are minimal, has revealed itself as essential for the correct calibration of the proposed models.

6. Future work

Experimental testing of the construction system outlined in this paper has yielded successful results for the presented composite, doubly-curved shells. Nonetheless, the applicability of this technique extends far beyond that, encompassing a broader range of structures, such as long-span, free-form or non-funicular shells. Regarding the latter, further experimental and numerical research is planned on doubly-curved, non-funicular, composite shells, for which the construction process should be carefully planned considering the tile vault's compression-only limitation when serving as formwork for the reinforced concrete. In respect of this purpose, the definition of the Finite Element model presented in this paper is regarded as an essential milestone.

Future work will also be aimed at studying diverse loading cases and, specifically, at better understanding and quantifying the influence of eventual abutment's relative displacements in the performance of such structures, with special attention to the comparison between the plain masonry shell and the composite system.

CRediT authorship contribution statement

David López López: Conceptualization, Methodology, Software, Validation, Formal analysis, Investigation, Resources, Data curation, Writing – original draft, Writing – review & editing, Visualization, Supervision, Project administration, Funding acquisition. **Ernest Bernat-Maso:** Validation, Investigation, Resources, Data curation, Writing – review & editing. **Savvas Saloustros:** Software, Validation, Formal analysis, Resources, Writing – review & editing. **Lluís Gil:** Validation, Investigation, Resources, Data curation, Writing – review & editing. **Pere Roca:** Conceptualization, Methodology, Software, Validation, Formal analysis, Investigation, Resources, Writing – review & editing, Supervision.

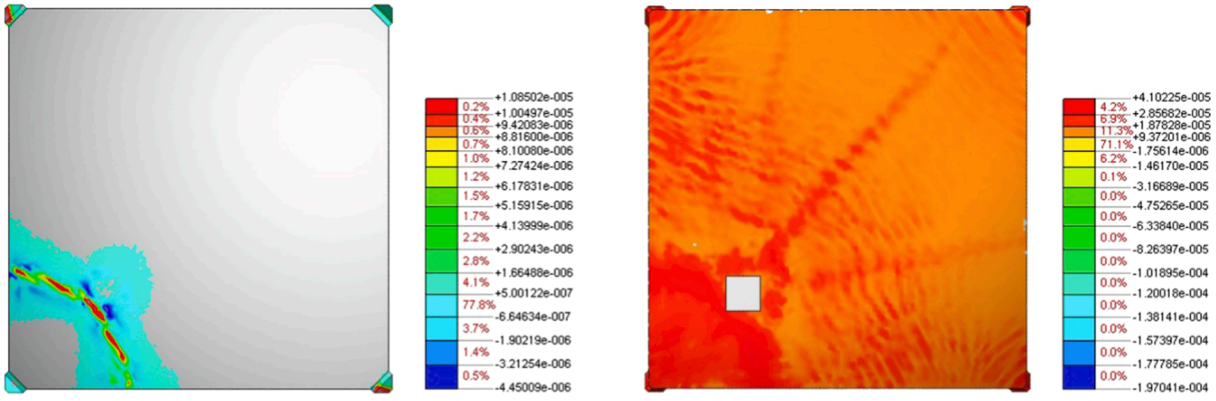

Fig. 22. FE model of the composite dome, crack width. Left) loading step at a displacement of 2.5 mm, showing from below the cracks at the intrados, and right) last loading step before failure, showing from above the radial-patterned cracks at the extrados.

Declaration of Competing Interest

The authors declare that they have no known competing financial interests or personal relationships that could have appeared to influence the work reported in this paper.

Data availability

Data will be made available on request.

Acknowledgements

This work was supported by the Swiss National Science Foundation (SNSF, project number P2EZP2_181591).

Second author is a Serra Húnter Fellow.

This research was also sponsored by the construction company URCOTEX, from which Josep Brazo, Antonio Haro and Albert Martí are especially acknowledged. The construction of the prototypes was carried out together with Jordi Domènech, to whom the authors are very thankful as well. Dr. Christian Escrig and Dr. Luis Mercedes, from the UPC's Laboratory for Technological Innovation in Structures and Materials (LITEM-CATMech), are acknowledged too for their support during the load tests' setup and during construction respectively.

The authors are likewise thankful to Dr. Diego Aponte and Prof. Dr. Marilda Barra (UPC) for their help in the development of the concrete's recipe and their valuable advice in this regard.

References

[1] Truñó Á. Construcción de bóvedas tabicadas; 1951.
[2] González Moreno-Navarro JL. La bóveda tabicada: Pasado y futuro de un elemento de gran valor patrimonial. Truñó, A. Construcción de bóvedas tabicadas. Madrid: Instituto Juan de Herrera 2004:11–60.
[3] Guastavino OJ. Vaulting: The Art of Structural Tile. Princeton Architectural Press; 2010.
[4] Fatta G, Campisi T, Vinci C. Timbrel vaults in Sicily: analysis of a little-known construction technique. Construct History 2016;31:107–32.
[5] Fuentes González P, Wouters I. Brick Vaults and Beyond: The Transformation of a Historical Structural System from 1750 to 1970. Instituto Juan de Herrera, Vrije Universiteit Brussel. Madrid: Taylor & Francis; 2021.
[6] Fuentes P. Auguste Fabre and the Construction of Tile Vaults in France. The Industrialization of a Traditional Technique. Int J Archit Herit 2022;16:1496–515. https://doi.org/10.1080/15583058.2021.1894504.
[7] Huerta FS. Las bóvedas tabicadas en Alemania: la larga migración de una técnica constructiva Actas del Segundo Congreso Internacional Hispanoamericano, Noveno Nacional, de Historia de la Construcción 2017;vol. 2:759–72.
[8] Almagro A. On the origin of certain vaults without formwork: Iranian timbrel vaults. History of Construction Cultures Volume 1, CRC Press; 2021.
[9] Costa Rosado A. Types and uses of vaults and timbrel vaults in Interior Alentejo: Data for a typological study. History of Construction Cultures Volume 1, CRC Press; 2021.
[10] Murphy E, Michiels D, Trelstad D. Forging the link among shape, formwork, and mortar assemblies in Guastavino vaulting. History of Construction Cultures Volume 1, CRC Press; 2021.
[11] López López D, Van Mele T, Block P. Tile vaulting in the 21st century. Inf Constr 2016;68:e162. https://doi.org/10.3989/ic.15.169.m15.
[12] Ramage MH, Ochsendorf J, Rich P, Bellamy JK, Block P. Design and Construction of the Mapungubwe National Park Interpretive Centre. South Africa ATDF J: Architecture 2010;7:14–23.
[13] Block P, Dejong M, Davis L, Ochsendorf J. Tile vaulted systems for low-cost construction in Africa. ATDF J 2010;7:4–13.
[14] De Wolf C, Ramage M, Ochsendorf J. Low Carbon Vaulted Masonry Structures. J Int Assoc Shell Spatial Struct 2016;57:275–84. https://doi.org/10.20898/j.iass.2016.190.854.
[15] Davis L, Rippmann M, Pawlofsky T, Block P. Innovative funicular tile vaulting: A prototype vault in Switzerland. Struct Eng 2012:46–56.
[16] López López D, Domènech Rodríguez M, Palumbo FM. "Brick-topia", the thin-tile vaulted pavilion. Case Stud Struct Eng 2014;2:33–40. https://doi.org/10.1016/j.csse.2014.09.001.
[17] Block P, Bayl-Smith M, Schork T, Bellamy J, Pigram D. Ribbed tile vaulting: Innovation through two design-build workshops. Fabricate: Negotiating Design Making, gta-Verlag 2014:22–9.
[18] Ramage M, Hall TJ, Gatóo A, Al Asali MW. Rwanda Cricket Stadium: Seismically stabilised tile vaults. Structures 2019;18:2–9. https://doi.org/10.1016/j.istruc.2019.02.004.
[19] Heyman J. The stone skeleton. Int J Solids Struct 1966;2:249–79.
[20] Andreu A, Gil L, Roca P. Computational Analysis of Masonry Structures with a Funicular Model. J Eng Mech 2007;133:473–80. https://doi.org/10.1061/(ASCE)0733-9399(2007)133:4(473).
[21] Block P, Lachauer L. Three-Dimensional (3D) Equilibrium Analysis of Gothic Masonry Vaults. Int J Arch Heritage 2014;8:312–35. https://doi.org/10.1080/15583058.2013.826301.
[22] Block P, Ciblac T, Ochsendorf J. Real-time limit analysis of vaulted masonry buildings. Comput Struct 2006;84:1841–52. https://doi.org/10.1016/j.compstruc.2006.08.002.
[23] Fraternali F. A thrust network approach to the equilibrium problem of unreinforced masonry vaults via polyhedral stress functions. Mech Res Commun 2010;37:198–204. https://doi.org/10.1016/j.mechrescom.2009.12.010.
[24] Bertolesi E, Milani G, Carozzi FG, Poggi C. Ancient masonry arches and vaults strengthened with TRM, SRG and FRP composites: Numerical analyses. Compos Struct 2018;187:385–402. https://doi.org/10.1016/j.compstruct.2017.12.021.
[25] Alexakis H, Makris N. Hinging Mechanisms of Masonry Single-Nave Barrel Vaults Subjected to Lateral and Gravity Loads. J Struct Eng 2017;143:04017026. https://doi.org/10.1061/(ASCE)ST.1943-541X.0001762.
[26] Chiozzi A, Milani G, Grillanda N, Tralli A. A fast and general upper-bound limit analysis approach for out-of-plane loaded masonry walls. Meccanica 2018;53:1875–98. https://doi.org/10.1007/s11012-017-0637-x.
[27] Chiozzi A, Milani G, Tralli A. A Genetic Algorithm NURBS-based new approach for fast kinematic limit analysis of masonry vaults. Comput Struct 2017;182:187–204. https://doi.org/10.1016/j.compstruc.2016.11.003.
[28] Chiozzi A, Milani G, Tralli A. Fast Kinematic Limit Analysis of FRP-Reinforced Masonry Vaults. I: General Genetic Algorithm–NURBS–Based Formulation. J Eng Mech 2017;143:04017071. 10.1061/(ASCE)EM.1943-7889.0001267.
[29] Milani G. Upper bound sequential linear programming mesh adaptation scheme for collapse analysis of masonry vaults. Adv Eng Softw 2015;79:91–110. https://doi.org/10.1016/j.advengsoft.2014.09.004.
[30] Dinani AT, Destro Bisol G, Ortega J, Lourenço PB. Structural Performance of the Esfahan Shah Mosque. J Struct Eng 2021;147:05021006. https://doi.org/10.1061/(ASCE)ST.1943-541X.0003108.
[31] Saloustros S, Pelà L, Roca P, Portal J. Numerical analysis of structural damage in the church of the Poblet Monastery. Eng Fail Anal 2015;48:41–61. https://doi.org/10.1016/j.engfailanal.2014.10.015.
[32] Creazza G, Matteazzi R, Saetta A, Vitaliani R. Analyses of Masonry Vaults: A Macro Approach based on Three-Dimensional Damage Model. J Struct Eng 2002;128:646–54. https://doi.org/10.1061/(ASCE)0733-9445(2002)128:5(646).
[33] Oñate E, Hanganu A, Barbat A, Oller S, Vitaliani R, Saetta A, et al. Structural analysis and durability assesment of historical constructions using a finite element damage model. Structural analysis of historic construction: Possibilities of numerical and experimental techniques. CIMNE 1995:189–224.
[34] Atamturktur S, Sevim B. Seismic Performance Assessment of Masonry Tile Domes through Nonlinear Finite-Element Analysis. J Perform Constr Facil 2012;26:410–23. https://doi.org/10.1061/(ASCE)CF.1943-5509.0000243.
[35] Pantò B, Cannizzaro F, Caddemi S, Caliò I, Chácara C, Lourenço PB. Nonlinear Modelling of Curved Masonry Structures after Seismic Retrofit through FRP Reinforcing. Buildings 2017;7:79. https://doi.org/10.3390/buildings7030079.
[36] D'Altri AM, De Miranda S, Castellazzi G, Sarhosis V, Hudson J, Theodossopoulos D. Historic Barrel Vaults Undergoing Differential Settlements. Int J Arch Heritage 2020;14:1196–209. https://doi.org/10.1080/15583058.2019.1596332.
[37] Bianchini N, Mendes N, Calderini C, Lourenço PB. Modelling of the dynamic response of a reduced scale dry joints groin vault. J Build Eng 2023;66:105826. https://doi.org/10.1016/j.jobe.2023.105826.
[38] Milani G, Rossi M, Calderini C, Lagomarsino S. Tilting plane tests on a small-scale masonry cross vault: Experimental results and numerical simulations through a heterogeneous approach. Eng Struct 2016;123:300–12. https://doi.org/10.1016/j.engstruct.2016.05.017.
[39] López López D, Van Mele T, Block P. The combination of tile vaults with reinforcement and concrete. Int J Arch Heritage 2019;13:782–98. https://doi.org/10.1080/15583058.2018.1476606.
[40] López López D, Roca P, Liew A, Van Mele T, Block P. Tile vaults as integrated formwork for reinforced concrete: Construction, experimental testing and a method for the design and analysis of two-dimensional structures. Eng Struct 2019;188:233–48. https://doi.org/10.1016/j.engstruct.2019.03.034.
[41] López López D, Bernat-Maso E, Gil L, Roca P. Experimental testing of a composite structural system using tile vaults as integrated formwork for reinforced concrete. Constr Build Mater 2021;300:123974. https://doi.org/10.1016/j.conbuildmat.2021.123974.
[42] Bertolesi E, Torres B, Adam JM, Calderón PA, Moragues JJ. Effectiveness of Textile Reinforced Mortar (TRM) materials for the repair of full-scale timbrel masonry cross vaults. Eng Struct 2020;220:110978. https://doi.org/10.1016/j.engstruct.2020.110978.
[43] Bertolesi E, Milani G, Adam JM, Calderón PA. 3D Advanced numerical modelling of a Catalan-layered masonry vault unreinforced and reinforced with glass-TRM materials and subjected to vertical support movements. Eccomas Proceedia COMPDYN, Athens, Greece: 2021, p. 415–22.
[44] Dejong M, Ramage M, Travers B, Terry S. Testing and Analysis of Geogrid-reinforced Thin-shell Masonry. Proceedings of the 35th Annual Symposium of IABSE / 52nd Annual Symposium of IASS / 6th International Conference on Space Structures, London, United Kingdom: 2011.
[45] Ramage M, Dejong M. Design and Construction of Geogrid-reinforced Thin-shell Masonry. Proceedings of the 35th Annual Symposium of IABSE / 52nd Annual Symposium of IASS / 6th International Conference on Space Structures, London, United Kingdom: 2011.

[46] Ramage MH, Gatóo A, Al Asali MW. Complex Simplicity—Design of Innovative Sustainable Thin-Shell Masonry Structures. In: Milani G, Sarhosis V, editors. From Corbel Arches to Double Curvature Vaults: Analysis, Conservation and Restoration of Architectural Heritage Masonry Structures. Cham: Springer International Publishing; 2022. p. 257–81. https://doi.org/10.1007/978-3-031-12873-8_10.
[47] Castori G, Borri A, Corradi M. Behavior of thin masonry arches repaired using composite materials. Compos B Eng 2016;87:311–21. https://doi.org/10.1016/j.compositesb.2015.09.008.
[48] Corradi M, Castori G, Borri A. A new method for strengthening tiled vaults: "Reinforced Catalan vaulting". 9th International Masonry Conference 2014 in Guimarães. 2014.
[49] Savino V, Franciosi M, Viviani M. Engineering and analyses of a novel Catalan vault. Eng Fail Anal 2023;143:106841. https://doi.org/10.1016/j.engfailanal.2022.106841.
[50] Al Asali MW, Couret DG, Ramage MH. Beyond the National Art Schools: Thin-Tile Vaulting in Cuba after the Revolution. J Soc Archit Hist 2021;80:321–45. https://doi.org/10.1525/jsah.2021.80.3.321.
[51] Del Curto D, Celli S. The Treachery of Images: Redefining the Structural System of Havana's National Art Schools. Sustainability 2021;13:3767. https://doi.org/10.3390/su13073767.
[52] Douglas I, Napolitano RK, Garlock M, Glisic B. Cuba's National School of Ballet: Redefining a structural icon. Eng Struct 2020;204:110040. https://doi.org/10.1016/j.engstruct.2019.110040.
[53] Douglas I, Napolitano R, Garlock M, Glisic B. Reconsidering the Vaulted Forms of Cuba's National School of Ballet. In: Aguilar R, Torrealva D, Moreira S, Pando MA, Ramos LF, editors. Structural Analysis of Historical Constructions. Cham: Springer International Publishing; 2019. p. 2150–8. https://doi.org/10.1007/978-3-319-99441-3_231.
[54] Hughes M, Celli S, Heubner C, Garlock M, Ottoni F, Del Curto D, et al. Nonlinear Finite-Element Analysis for Structural Investigation and Preservation of Reinforced Hybrid Thin Tile-Concrete Domes of the Historic School of Ballet Classrooms in Havana. Cuba J Performance Constructed Facilities 2023;37:04022074. https://doi.org/10.1061/(ASCE)CF.1943-5509.0001780.
[55] Hughes M, Heubner C, Celli S, Garlock M, Ottoni F, Del Curto D, et al. Shrouded by time and tile: a structural investigation for preservation of Cuba's historic School of Ballet classroom and theatre domes. Proceedings of the IASS Annual Symposium 2020/21 and the 7th International Conference on Spatial Structures. Inspiring the Next Generation, Guilford, UK: S.A Behnejad, G. A. R. Parke and O.A.Samavati (eds.); 2021, p. 1029–40.
[56] López López D, Roca P, Liew A, Méndez Echenagucia T, Van Mele T, Block P. A three-dimensional approach to the Extended Limit Analysis of Reinforced Masonry. Structures 2022;35:1062–77. https://doi.org/10.1016/j.istruc.2021.06.013.
[57] Block P, Ochsendorf J. Thrust Network Analysis: A New Methodology for Three-Dimensional Equilibrium. J Int Assoc Shell Spatial Struct 2007;48:8.
[58] CEN. EN 1015: Methods of test for mortar for masonry ;2000.
[59] CEN. EN 12390: Testing Hardened Concrete; 2001.
[60] CEN. Eurocode 6: Design of masonry structures. EN 1996-1-1: 2005; 2005.
[61] Ministerio de Fomento de España. EHE, Instrucción de hormigón structural; 1999.
[62] CEN. EN 197: Cement. Part 1: Composition, specifications and conformity criteria for common cements; 2011.
[63] CEN. EN ISO 15630: Steel for the reinforcement and prestressing of concrete. Test methods. Part 1: Reinforcing bars, wire rod and wire; 2002.
[64] López López D. Tile Vaults as Integrated Formwork for Concrete Shells: Construction, Experimental Testing, Structural Analysis and Design. Doctoral Thesis. ETH Zurich; 2019. 10.3929/ethz-b-000417993.
[65] Lawrence SJ, Cao HT. An experimental study of the interface between brick and mortar. Proceedings of the 4th North American Masonry Conference, Los Ángeles; 1987, p. 1–14.
[66] Venkatarama Reddy BV, Lal R, Nanjunda Rao KS. Enhancing Bond Strength and Characteristics of Soil-Cement Block Masonry. J Mater Civ Eng 2007;19:164–72. https://doi.org/10.1061/(ASCE)0899-1561(2007)19:2(164).
[67] Venu Madhava Rao K, Venkatarama Reddy BV, Jagadish KS. Flexural bond strength of masonry using various blocks and mortars. Mat Struct 1996;29:119–24. https://doi.org/10.1007/BF02486202.
[68] Sarangapani G, Venkatarama Reddy BV, Jagadish KS. Brick-Mortar Bond and Masonry Compressive Strength. J Mater Civ Eng 2005;17:229–37. https://doi.org/10.1061/(ASCE)0899-1561(2005)17:2(229).
[69] Sinha BP. Model studies related to load bearing brickwork. University of Edinburgh, n.d.
[70] Groot C. Effects of water on mortar-brick bond. Delft University of Technology; 1993.
[71] Thamboo JA, Dhanasekar M, Yan C. Flexural and shear bond characteristics of thin layer polymer cement mortared concrete masonry. Constr Build Mater 2013;46:104–13. https://doi.org/10.1016/j.conbuildmat.2013.04.002.
[72] Thamboo JA, Dhanasekar M. Characterisation of thin layer polymer cement mortared concrete masonry bond. Constr Build Mater 2015;82:71–80. https://doi.org/10.1016/j.conbuildmat.2014.12.098.
[73] Lawrence SJ, Page AW. Bond studies in masonry. Proceedings of the 10th International Brick and Block Masonry Conference, Calgary, Canada: University of Calgary; 1994, p. 909–17.
[74] CEN. Eurocode 2: Design of concrete structures. EN 1992-1-1: 2004; 2004.
[75] CEN. Eurocode 1: Actions on structures - Part 1-1: General actions - Densities, self-weight, imposed loads for buildings. EN 1991-1-1: 2002; 2002.
[76] López López D, Bernat-Maso E, Gil L, Roca P. Experimental testing of tile vaults. Brick and Block Masonry - From Historical to Sustainable Masonry, CRC Press; 2020.
[77] DIANA FEA. User's Manual - Release 10.2; 2017.
[78] Selby RG, Vecchio FJ. Three-dimensional constitutive relations for reinforced concrete. Toronto: University of Toronto, Dept. of Civil Engineering; 1993.
[79] Feenstra PH. Computational Aspects of Biaxial Stress in Plain and Reinforced Concrete. Doctoral thesis. Delft University Press; 1993.
[80] Saloustros S. Tracking localized cracks in the computational analysis of masonry structures. Universitat Politècnica de Catalunya; 2017. Doctoral thesis.
[81] Comite Euro-International Du Beton. CEB-FIP MODEL CODE 1990: DESIGN CODE 1993.
[82] Lourenço PB. Recent advances in masonry modelling: micromodelling and homogenisation. Multiscale Modeling in Solid Mechanics, vol. Volume 3, IMPERIAL COLLEGE PRESS; 2009, p. 251–94. 10.1142/9781848163089_0006.
[83] Ministerio de Fomento de España. Código Técnico de la Edificación, CTE. Documento Básico, Seguridad Estructural, Acero; 2007.
[84] Červenka V, Jendele L, Červenka J. ATENA Program Documentation. Part 1. Theory; 2018.